

DFT-Based Study of the Structure, Stability, and Spectral and Optical Properties of Gas-Phase NbMg_n (n = 2–12) Clusters

Xiao-Feng Gao, Guang-Hui Liu, Xian-Kai Hu, Lan-Li Chen, Ben-Chao Zhu,* Ding-Shan Zheng,* and Yan-Hua Liao*



Cite This: *ACS Omega* 2023, 8, 41391–41401



Read Online

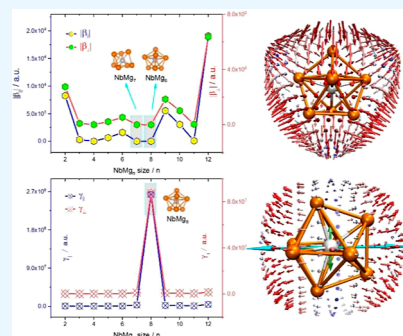
ACCESS |

Metrics & More

Article Recommendations

Supporting Information

ABSTRACT: Gas-phase NbMg_n (n = 2–12) clusters were fully searched by CALYPSO software, and then the low-energy isomers were further optimized and calculated under DFT. It is shown that the three lowest energy isomers of NbMg_n (n = 3–12) at each size are grown from two seed structures, i.e., tetrahedral and pentahedral structures, and the transition size occurs at the NbMg₈ cluster. Interestingly, the relative stability calculations of the NbMg₈ cluster ground-state isomer stand out under the examination of several parameters' calculations. The charge-transfer properties of the clusters of the ground-state isomers of various sizes had been comprehensively investigated. In order to be able to provide data guidance for future experimental probing of these ground-state clusters, this work also predicted infrared and Raman spectra at the same level of theoretical calculations. The results show that the multippeak nature of the IR and Raman spectra predicts that it is difficult to distinguish them directly. Finally, the optical properties of these clusters were investigated by calculating the static linear, second-order nonlinear, and third-order nonlinear coefficients. Importantly and interestingly, the NbMg₈ cluster was shown to have superior nonlinear optical characteristics to all other clusters; thus, it is a powerful candidate for a potentially ultrasensitive nonlinear optical response device for some special purpose.



1. INTRODUCTION

In the last decades, the study of atomic clusters has attracted increasing interest from researchers.^{1–3} It is because, on the one hand, they are always size-dependent below a critical size and therefore have many size-dependent physical and chemical properties. On the other hand, the atomic clusters often show peculiar structures and are thus potential units for some functional nanomaterials, which has led to great importance in the field of theoretical research of nanomaterials.^{4,5} The study of various gas-phase or ligand-protected liquid-phase atomic clusters has been extensively reported, e.g., metallic atomic clusters such as gold,^{6,7} silver,^{8–10} molybdenum,¹¹ cobalt,^{12–16} copper,^{17,18} nickel,^{19–21} magnesium,^{22,23} etc., and nonmetallic objects such as carbon,^{24–26} boron,^{27,28} and silicon.^{29,30} These studies have greatly advanced the application of atomic clusters in catalysis, combustion, crystal growth, nucleation and solidification, phase change, sol–gel, thin-film formation, and sputtering. Interestingly, the study of doped atomic clusters can also provide theoretical explanations for the physical and chemical properties of some alloying materials, e.g., first-principles studies of Zn–Mg variable-component clusters have shown that Mg₂Zn₁₁ and MgZn₂ are the best candidates for optimizing the corrosion protection of zinc–magnesium alloys. Such studies are of great importance as they greatly contribute to research and development in the field of nanomaterials.³¹

It is well-known that materials science always classifies materials into three categories, namely, 3-dimensional bulk materials, 2-dimensional planar materials, and 1-dimensional linear materials, so that clusters in sizes smaller than nanoparticles are usually referred to as 0-dimensional.¹ However, it should be emphasized that atomic clusters have various structures, and it is these structures that are responsible for their amazing properties. The key task in clusters research is to obtain their structures, and the usual research route is to conduct relatively low-cost theoretical studies to calculate and predict some spectral properties first and then to verify them by more costly experiments. Atomic clusters of a specific atomic number arranged spatially according to different orientations have different configurations, and their energies obviously differ. Therefore, based on some smart algorithm, atomic clusters are studied to obtain structures by performing global optimization and conformational search of clusters to find the lowest-energy isomers on their potential energy surfaces.^{32–34} These globally optimized low-energy isomers are

Received: July 16, 2023

Revised: October 9, 2023

Accepted: October 12, 2023

Published: October 24, 2023



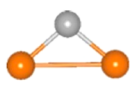
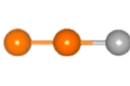

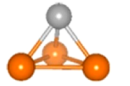
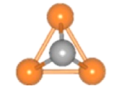
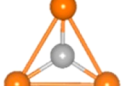
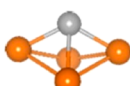


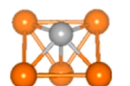

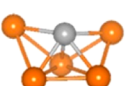
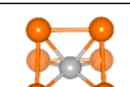
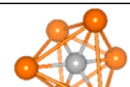
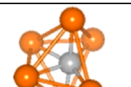
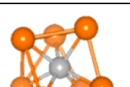
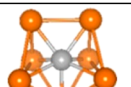
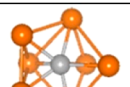
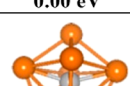
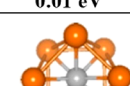
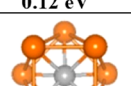

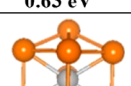
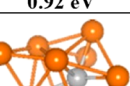
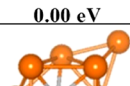
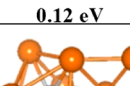
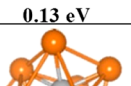
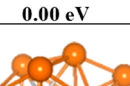
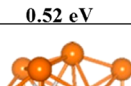
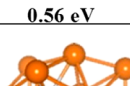
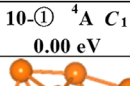
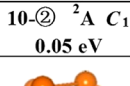
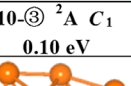

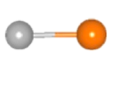
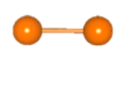
					
2-① ${}^6A_1 C_{6v}$ 0.00 eV	2-② ${}^4\Sigma_g C_{\infty v}$ 0.39 eV	2-③ ${}^4B_2 C_{2v}$ 0.42 eV	3-① ${}^6A_1 C_{3v}$ 0.00 eV	3-② ${}^4A_1 C_{3v}$ 0.31 eV	3-③ ${}^6A_1' D_{3h}$ 0.35 eV
					
4-① ${}^6A_1 C_{2v}$ 0.00 eV	4-② ${}^6A' C_s$ 0.10 eV	4-③ ${}^4B_2 C_{2v}$ 0.28 eV	5-① ${}^6A_1 C_{3v}$ 0.00 eV	5-② ${}^4A_1 C_{5v}$ 0.06 eV	5-③ ${}^6A C_1$ 0.10 eV
					
6-① ${}^2A C_1$ 0.00 eV	6-② ${}^2A' C_s$ 0.01 eV	6-③ ${}^2A_1 C_{2v}$ 0.12 eV	7-① ${}^2A C_1$ 0.00 eV	7-② ${}^4A C_1$ 0.63 eV	7-③ ${}^6A C_1$ 0.92 eV
					
8-① ${}^2B_2 D_{2d}$ 0.00 eV	8-② ${}^2A_1 C_{4v}$ 0.12 eV	8-③ ${}^4B_2 D_{4d}$ 0.13 eV	9-① ${}^4A C_1$ 0.00 eV	9-② ${}^4B_1 C_{2v}$ 0.52 eV	9-③ ${}^6A' C_s$ 0.56 eV
					
10-① ${}^4A C_1$ 0.00 eV	10-② ${}^2A C_1$ 0.05 eV	10-③ ${}^2A C_1$ 0.10 eV	11-① ${}^2A C_1$ 0.00 eV	11-② ${}^4A' C_s$ 0.15 eV	11-③ ${}^6A' C_s$ 0.32 eV
					
12-① ${}^2A C_1$ 0.00 eV	12-② ${}^4A C_1$ 0.16 eV	12-③ ${}^2A'' C_s$ 0.25 eV	Nb	Mg	Nb-Mg
					Mg-Mg

Figure 1. Isomer structures of $NbMg_n$ (①, ②, and ③) ($n = 2-12$) clusters; ①, ②, and ③ mean the lowest order of isomer energy. The energy (in eV) under each isomer is the energy difference relative to that of the ground-state isomer.

often theoretically predicted and thus require experimental confirmation. Various spectral properties, such as IR, Raman, UV–vis, and photoelectron spectra, are powerful data to guide experimental verification. For example, these spectral values were calculated theoretically for magnesium-based clusters,^{35–40} silicon-based clusters,^{41,42} and boron-based clusters.^{43,44} These studies, although they are mostly carried out theoretically and have no possibility of being experimentally confirmed in the short term, can, on the one hand, fill the database of atomic clusters and, on the other hand, they are basic scientific problems that must be clarified for people to understand the macroscopic structure of atoms aggregated into clusters to blocks. Therefore, the study of clusters with a wide range of material applicabilities, including their spectroscopic studies, is always favored by researchers. Interestingly, despite the industrial importance of niobium⁴⁵ and magnesium,^{46,47} the study of niobium-doped magnesium clusters has not been reported. Specifically, this work doped single neutral Nb atom into Mg_n ($n = 2-12$) clusters. The geometric growth mechanism, relative stability, and various spectral properties of $NbMg_n$ ($n = 2-12$) clusters of each size will be

systematically investigated. In addition, the linear and non-linear optical (NLO) properties of the $NbMg_n$ ($n = 2-12$) ground-state isomers have also been fully studied.

2. COMPUTATIONAL METHODS

The search for all initial low-lying energy isomers' structures of $NbMg_n$ ($n = 2-12$) on the global potential energy surface was performed by CALYPSO software.⁴⁸ CALYPSO is a useful tool to efficiently predict the structures of crystals,^{49,50} clusters,^{51–56} or functional materials under external environments (e.g., pressure),^{57,58} given only the chemical composition of the compound. The initial 50 structures were randomly generated by symmetric constraints, and subsequently, 80% of the previous-generation structures with high fitness were selected using the particle swarm optimization algorithm to generate new structures, while the remaining 20% were randomly generated. Considering the similar structures with respect to bonding characteristics, we excluded them using the bond characterization matrices. The structure search was performed for 20 generations with 50 structures per generation. Thus, a total of 1000 test structures were

Table 1. Bonding Energy per Atom (E_b), the Second-Order Difference Energy (Δ_2E), HOMO–LUMO Energy Gap (E_{gap}), the Lowest Vibrational Frequency, VIP, and VEA in the Ground-State Isomers of NbMg_n ($n = 2–12$) Clusters

isomer	E_b (eV)	Δ_2E (eV)	$E_{\text{gap}}-\alpha$ (eV)	$E_{\text{gap}}-\beta$ (eV)	lowest Freq (cm^{-1})	VIP (eV)	VEA (eV)	KS-gap (eV)	F-gap (eV)
NbMg_2	0.35		1.31	3.38	33	5.29	0.78	4.69	4.51
NbMg_3	0.53	0.15	1.40	2.56	86	5.48	1.19	3.96	4.29
NbMg_4	0.61	0.14	1.41	2.22	64	5.30	1.31	3.63	3.99
NbMg_5	0.64	−0.20	1.59	1.56	44	5.17	0.98	3.14	4.19
NbMg_6	0.69	−0.71	1.76	1.48	13	4.85	0.85	3.24	4.00
NbMg_7	0.81	0.71	1.11	2.15	18	4.25	1.21	3.26	3.05
NbMg_8	0.83	1.03	1.13	1.39	7	4.42	0.91	2.52	3.51
NbMg_9	0.74	−1.11	1.01	1.77	39	4.59	1.85	2.78	2.73
NbMg_{10}	0.77	−0.24	1.14	1.93	35	4.53	1.35	3.07	3.17
NbMg_{11}	0.81	0.38	1.05	1.11	11	4.39	1.32	2.17	3.07
NbMg_{12}	0.82		1.06	1.09	40	4.42	1.56	2.15	2.86

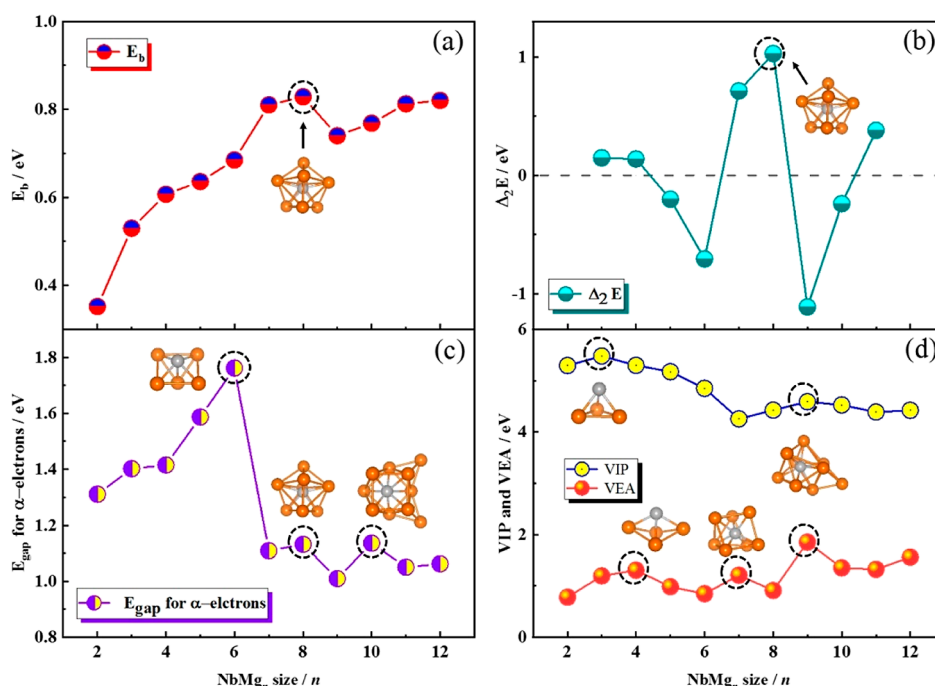


Figure 2. (a) E_b , (b) Δ_2E , and (c) E_{gap} for α electrons. (d) VIP and VEA in the ground-state isomers of NbMg_n ($n = 2–12$) clusters.

preoptimized for each NbMg_n using the b3pw91 functional⁵⁹ and a small 6-31G basis set⁶⁰ using the Gaussian09 program.⁶¹ For each size of NbMg_n , the 30 lowest-energy isomers were selected for the next stage of higher-level structural optimization calculations, which adopted the b3pw91 functional and the 6-311g(d) basis set⁶⁰ for Mg and the pseudopotential basis set lanl2dz⁶² for Nb. Since the NbMg_n cluster has a closed-shell layer structure for Mg_n and an open-shell layer for Nb, the 2,4,6, and 8 spin multiplicity states were optimized for each cluster separately. In addition, the simple harmonic vibration frequency calculations performed along with structural optimization require that no imaginary frequencies appear, ensuring that the obtained states correspond to local minima on the potential energy surface. This choice of calculation level is based on the previous successful studies of Mg-based clusters reported.^{35,36,52} Note that in all structural optimization calculations, a default convergence criterion of Gaussian 09 was used. The charge transfer characteristics of doped atom and host atom were analyzed through natural bond orbital (NBO) calculations.⁶³ When calculating the dipole moment, polarizability, and first

hyperpolarizability, the dispersion function [DFT-D3(BJ)] was considered,⁶⁴ while the dispersion correction basis set should be 6-311G+(d). The graphical representation of the unit spherical α polarization was implemented through Multiwfn software.⁶⁵

3. RESULTS AND DISCUSSION

3.1. Geometry Growth of NbMg_n ($n = 2–12$) Clusters.

The structures of the three lowest-energy states of each size cluster, $\text{NbMg}_n\text{-}\textcircled{1}$, $\text{NbMg}_n\text{-}\textcircled{2}$, and $\text{NbMg}_n\text{-}\textcircled{3}$, as well as point group symmetries, electronic states, and energy difference to the ground-state isomer, are shown in Figure 1. In addition, the atomic coordinates of the ground-state isomers of the NbMg_n ($n = 2–12$) cluster are given in Table S1 of the Supporting Information. Isomers 2- $\textcircled{1}$ (C_{6v} , 6A_1) and 2- $\textcircled{3}$ (C_{2v} , 4B_2) show the isosceles triangle structure. The Mg–Nb bond lengths of the two isomers are 2.80 and 2.86 Å, respectively, and the Mg–Nb–Mg bond angles are 98.2° and 67.3°, respectively. Isomer 2- $\textcircled{2}$ ($C_{\infty v}$, ${}^4\Sigma_g$) has a Mg–Mg–Nb linear structure, where the Mg–Mg and Mg–Nb distances are 3.29 and 2.94 Å, respectively. The second and third lowest-energy isomers of

Table 2. Natural Charge Population and Natural Electron Configuration Analysis on Nb Atoms in the Ground-State Isomers of NbMg_n (n = 2–12) Clusters

clusters	NCP–Nb (e)	NEC–Nb (e)
NbMg ₂	−0.57	[core]5s ^{0.91} 4d ^{4.43} 5p ^{0.23}
NbMg ₃	−1.13	[core]5s ^{1.03} 4d ^{4.54} 5p ^{0.53} 5d ^{0.01} 6p ^{0.02}
NbMg ₄	−1.88	[core]5s ^{1.14} 4d ^{4.90} 5p ^{0.77} 5d ^{0.01} 6p ^{0.06}
NbMg ₅	−3.31	[core]5s ^{1.11} 4d ^{5.80} 5p ^{1.34} 5d ^{0.03} 6p ^{0.03}
NbMg ₆	−5.23	[core]5s ^{0.89} 4d ^{6.88} 5p ^{2.43} 5d ^{0.02}
NbMg ₇	−6.82	[core]5s ^{1.41} 4d ^{7.49} 5p ^{2.91} 5d ^{0.01}
NbMg ₈	−7.48	[core]5s ^{1.83} 4d ^{7.61} 5p ^{3.03} 5d ^{0.01}
NbMg ₉	−5.76	[core]5s ^{1.39} 4d ^{6.58} 5p ^{2.76} 5d ^{0.02} 6p ^{0.01}
NbMg ₁₀	−6.81	[core]5s ^{1.15} 4d ^{7.58} 5p ^{3.05} 5d ^{0.02} 6p ^{0.01}
NbMg ₁₁	−7.68	[core]5s ^{1.79} 4d ^{7.72} 5p ^{3.16} 5d ^{0.01} 6p ^{0.01}
NbMg ₁₂	−7.52	[core]5s ^{1.59} 4d ^{7.76} 5p ^{3.16} 5d ^{0.01} 6p ^{0.01}

the NbMg₂ cluster are 0.38 and 0.42 eV higher than the energy of the ground-state isomer, respectively. For the NbMg₃ cluster, the ground-state and the second-lowest-energy isomers show similar tetrahedral structures. The 3-⊖(*D*_{3h}, ⁶A₁) isomer is an equilateral triangular structure (Mg–Mg distance of 4.91 Å), where the Nb atom is in the geometric center (Mg–Nb distance of 2.84 Å). The energy of the ground-state isomer of NbMg₃ is 0.31 and 0.35 eV lower than the second-lowest and third-lowest energy isomers, respectively. The structures of the three lowest-energy isomers of the NbMg₄ cluster are all based on the tetrahedral shape of 3-⊖ grown by the adsorption of one Mg atom in different orientations. The isomers 4-⊖(*C*_s, ⁶A') and 4-⊗(*C*_{2v}, ⁴B₂) have 0.10 and 0.28 eV higher energy than the ground-state isomer 4-⊖(*C*_{2v}, ⁶A₁), respectively. For the clusters NbMg₅, NbMg₆, NbMg₇, and 8-⊖(*D*_{2d}, ²B₂), the

structures of the isomers are obtained based on tetrahedral structure growth, except for the structure of isomer 5-⊖(*C*_{5v}, ⁴A₁), which is a tent type with a pentagonal bottom edge. Their energy differences relative to their own ground-state structures are distributed in the range of 0.01–0.93 eV. Starting from the 8-⊖ isomer, the shape of the NbMg_n (n = 9–12) cluster changes, and the structure of the tetrahedral basic unit is difficult to be observed directly. In some perspectives, they grow as a unit of a pentahedral structure. The 8-⊖ isomer appears to be special because its upper part is pentahedral and its lower part is tetrahedral, so we can identify it as a transformation node size for the structural change of the NbMg_n cluster. It is necessary to emphasize that this complex structure, which grows up in a pentahedral structure, sometimes presents a tower-like (such as BeMg₉⁶⁶) or yurt-like^{37,38} structure. Interestingly, isomers 8-⊖ and 8-⊗ have the similar quadrangular antiprism structures, which are the same as the structure of the lowest-energy isomers of the 4d-transition-metal atom X-doped Mg₈ host (X = Y, Zr, Nb, Mo, Tc, Ru, Rh, Pd, and Ag).⁶⁷ It should be noted, however, that our study shows that this structure is not the lowest-energy isomer of NbMg₈. In addition, NbMg_n (n = 8–12) cluster calculations show that their second-lowest and third-lowest isomers have energies in the range of 0.05–0.56 eV higher than their ground-state isomers.

In summary, our calculations show that in addition to the NbMg₂ clusters showing linear and planar structures, the structural growth of Nb atom-doped Mg_n (n = 3–12) clusters is based on the growth of tetrahedral and pentahedral structures, which can be regarded as two seed unit structures, as presented in Figure S1 of the Supporting Information. It is

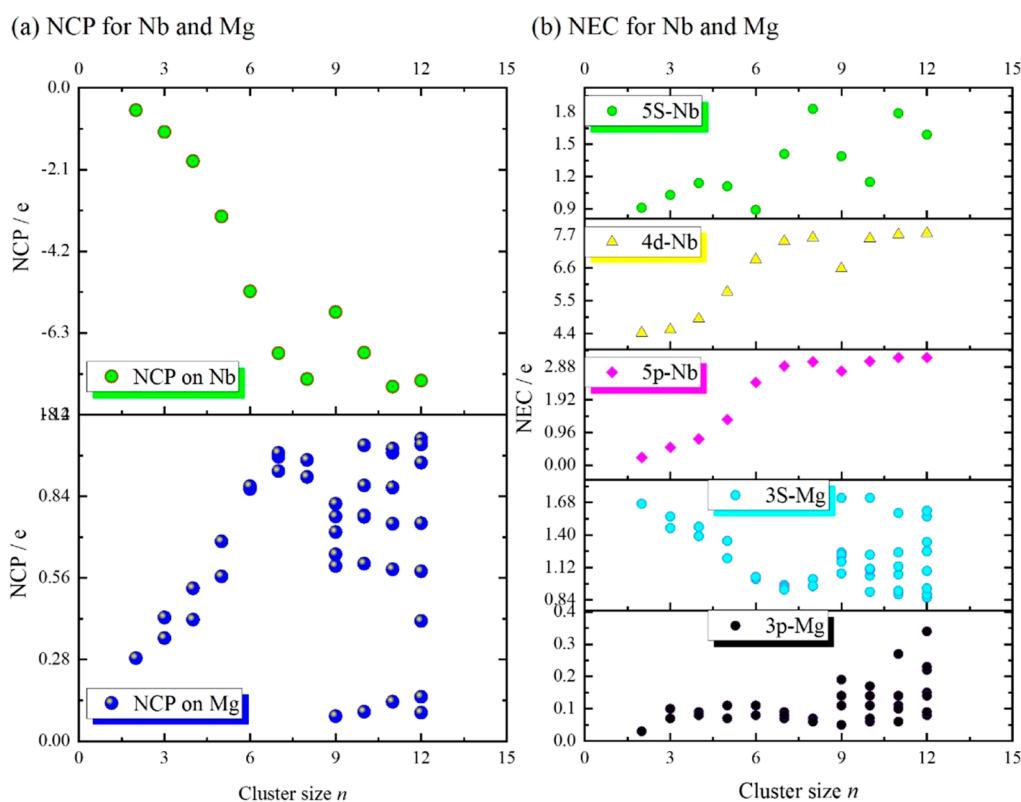


Figure 3. Charge transfer characteristics analysis: (a) NCP and (b) NEC for Nb and Mg atoms in the ground-state isomers of NbMg_n (n = 2–12) clusters.

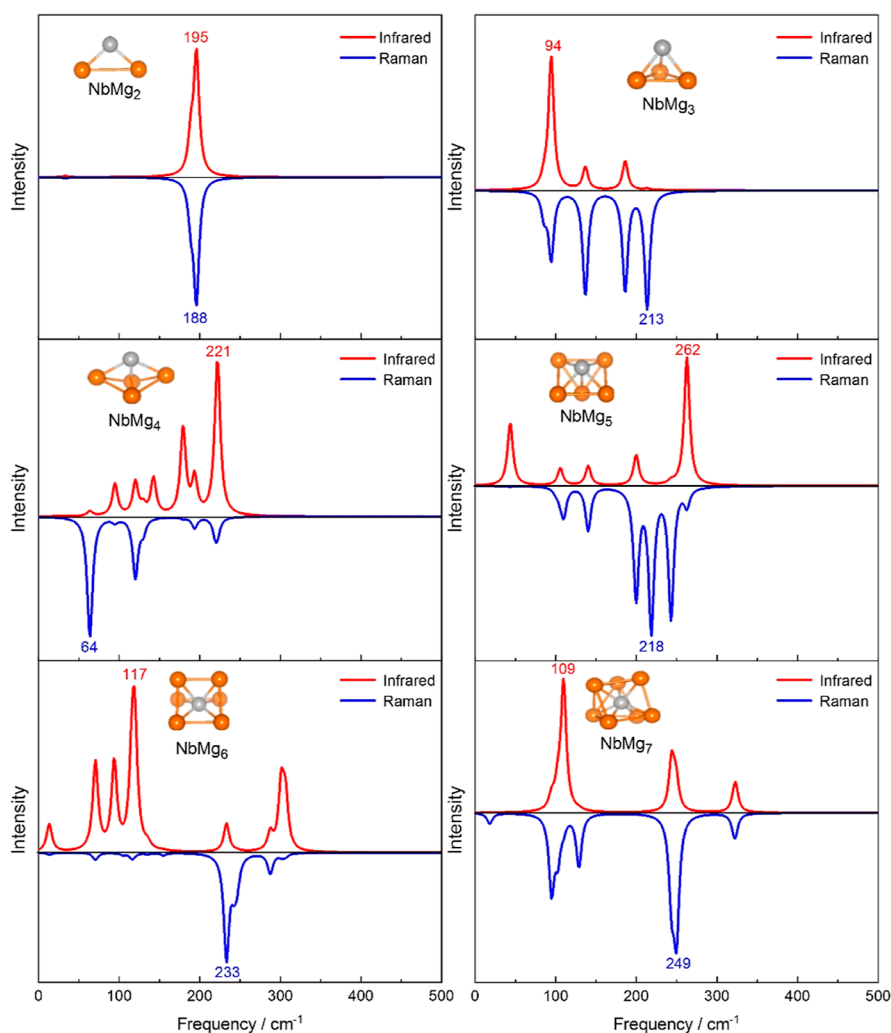


Figure 4. Theoretical calculation of IR and Raman spectra for the ground-state isomers for NbMg_n ($n = 2-7$) clusters.

interesting to note that the spin multiplicity of the small-sized NbMg_n ($n = 2-5$) ground-state isomer is 6, while those of the ground-state isomers of BeMg_n ,⁶⁶ GaMg_n ,^{37,38} and other Mg-based clusters are mostly 2.

3.2. Relative Stability Property of NbMg_n ($n = 2-12$) Clusters. Because the ground-state isomers are lowest in energy, it means they are more stable and worthy to be studied. The lowest vibrational frequencies of all of the ground-state clusters in Table 1 are greater than zero (no imaginary frequency), confirming that they are the local lowest-energy states on their potential energy surfaces. Since the stability of clusters varies with their size, it is extremely important to study the relative stability of the ground-state clusters. Information on the coordinates of all the ground-state isomers is given in Table S1 of the Supporting Information. Six energies, binding energy per atom (E_b), the second-order energy difference ($\Delta_2 E$), the energy gap between the highest occupied molecular orbital and lowest unoccupied molecular orbital (HOMO–LUMO E_{gap}), the vertical ionization potential (VIP), the vertical electron affinity (VEA) energy, and the fundamental energy gap (VIP–VEA), are commutated to study the relative stability of the ground-state isomers of NbMg_n ($n = 2-12$) clusters.

$$E_b(\text{NbMg}_n) = [E(\text{Nb}) + nE(\text{Mg}) - E(\text{NbMg}_n)] / (n + 1) \quad (1)$$

$$\Delta_2 E(\text{NbMg}_n) = E(\text{NbMg}_{n+1}) + E(\text{NbMg}_{n-1}) - 2E(\text{NbMg}_n) \quad (2)$$

$$E_{\text{gap}}(\text{NbMg}_n) = E_{\text{LUMO}}(\text{NbMg}_n) - E_{\text{HOMO}}(\text{NbMg}_n) \quad (3)$$

$$E_{\text{VIP}} = E_{\text{neutralstructure}}(\text{NbMg}_n^{+1}) - E_{\text{neutralstructure}}(\text{NbMg}_n) \quad (4)$$

$$E_{\text{VEA}} = E_{\text{neutralstructure}}(\text{NbMg}_n) - E_{\text{neutralstructure}}(\text{NbMg}_n^{-1}) \quad (5)$$

$$E_{\text{Fundamental-gap}} = \text{VIP} - \text{VEA} \quad (6)$$

The E in eqs 1–5 represents the energy of the substance in the brackets to its right, the -1 and $+1$ appearing in VIP and VEA are the charge properties of the corresponding clusters in the neutral structure, and $E_{\text{neutralstructure}}(\text{NbMg}_n)$ means the energy of the fixed neutral cluster structure.

Table 1 presents the results of these energy calculations, and they are shown graphically in Figures 2 and S1 in the Supporting Information. As shown in Figure 2a, the overall trend of the E_b curve of the lowest-energy state of NbMg_n ($n =$

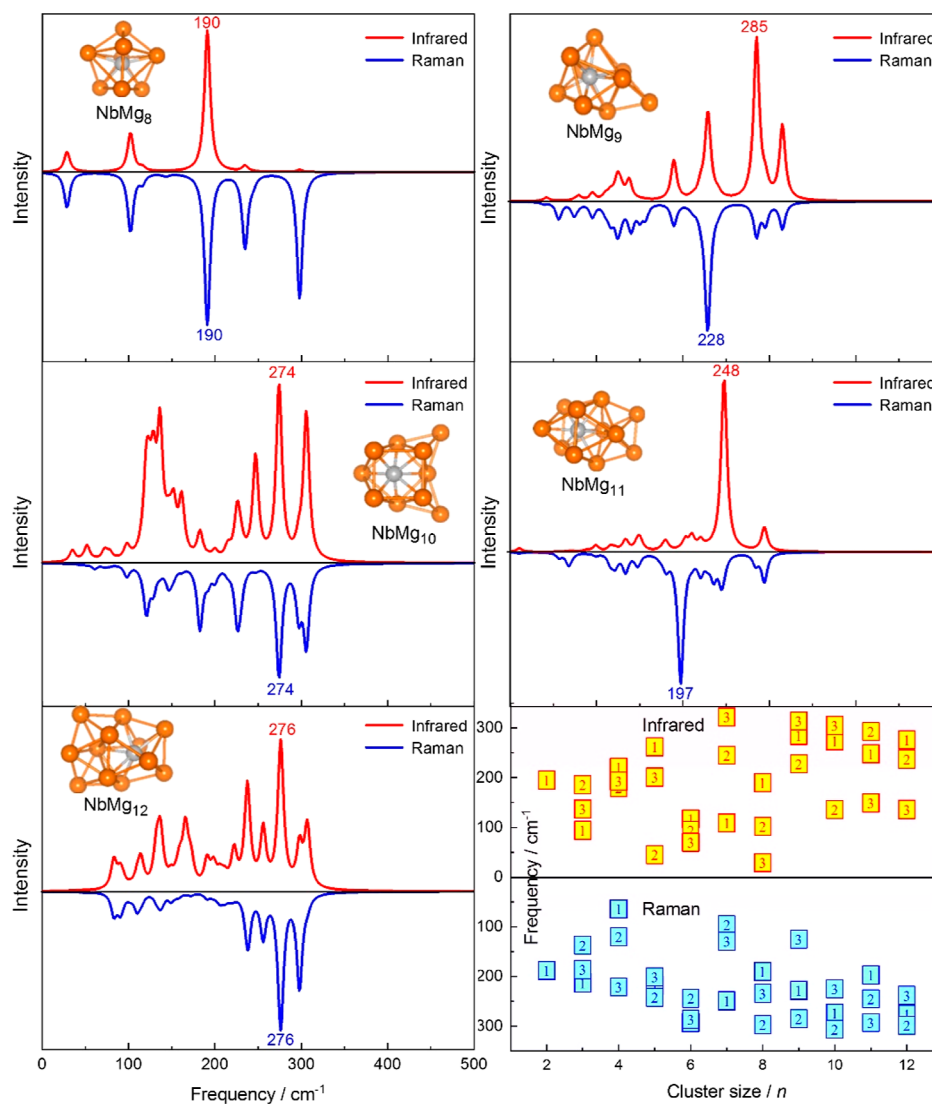


Figure 5. Theoretical calculation of IR and Raman spectra for the ground-state isomers for NbMg_n ($n = 8–12$) clusters.

2–12) clusters increases with increasing cluster size. The largest E_b value of 0.83 eV occurs at $n = 8$, indicating that it has higher relative stability than other clusters. As can be seen from eq 2, the $\Delta_2 E$ value is a parameter that measures the relative stability of a cluster with its neighbors, and its larger value indicates higher relative stability and vice versa. The $\Delta_2 E$ curve oscillates with cluster size in Figure 2b, and the maximum value of 1.03 eV is also observed at NbMg_8 . This indicates that the ground state of the NbMg_8 cluster has the highest relative stability. HOMO–LUMO E_{gap} values for α and β electrons are calculated and plotted in Figures 2c and S2 in the Supporting Information. The magnitude of the E_{gap} value is a useful parameter to reflect the chemical stability of clusters. On the one hand, for α -electrons, NbMg_6 has the largest E_{gap} value (1.76 eV). Locally, NbMg_8 and NbMg_{10} have higher stability than their neighboring clusters. On the other hand, for β -electrons, NbMg_2 has the largest E_{gap} value (3.38 eV), and NbMg_7 and NbMg_{10} have locally larger E_{gap} values. When considering the Kohn–Sham gap (KS-gap)⁶⁸ of the clusters, i.e., the sum of the α and β electronic contributions, Table 1 and Figure S3 in the Supporting Information reveal that the KS-gap values of the NbMg_n isomers are becoming smaller as a whole, with the KS-gap of NbMg_2 being the largest (4.69 eV),

and locally, NbMg_7 and NbMg_{10} are more stable than their neighboring clusters. Finally, for the energy values that reflect the ability of the cluster to gain and lose an electron, VIP and VEA were calculated separately. As shown in Table 1 and Figure 2d, both VIP and VEA values of the lowest energy state of NbMg_n ($n = 2–12$) clusters are positive, indicating that neutral NbMg_n clusters are required to absorb and release energy for ionization and affinity of one electron. It is shown that the NbMg_3 ground-state isomer possesses the largest VIP value of 5.29 eV, and locally, the NbMg_9 ground-state isomer has a VIP value of 4.59 eV larger than that of any of its neighbors. This suggests that both are more difficult to ionize relative to other clusters and thus more stable. The VEA curve shows that the NbMg_9 cluster has the largest affinity energy with a value of 1.85 eV, followed by NbMg_{12} with 1.56 eV. Locally, the VEA values of both NbMg_4 and NbMg_7 are larger than those of their neighboring clusters, suggesting that these clusters are more stable as they release more energy when gaining electrons. It can be safely concluded that the ground-state isomer of NbMg_9 presents a relatively remarkable stability in terms of the electron affinity and ionization. Since the difference between VIP and VEA is the Fundamental gap (F-gap) of the system, it is another useful parameter to measure

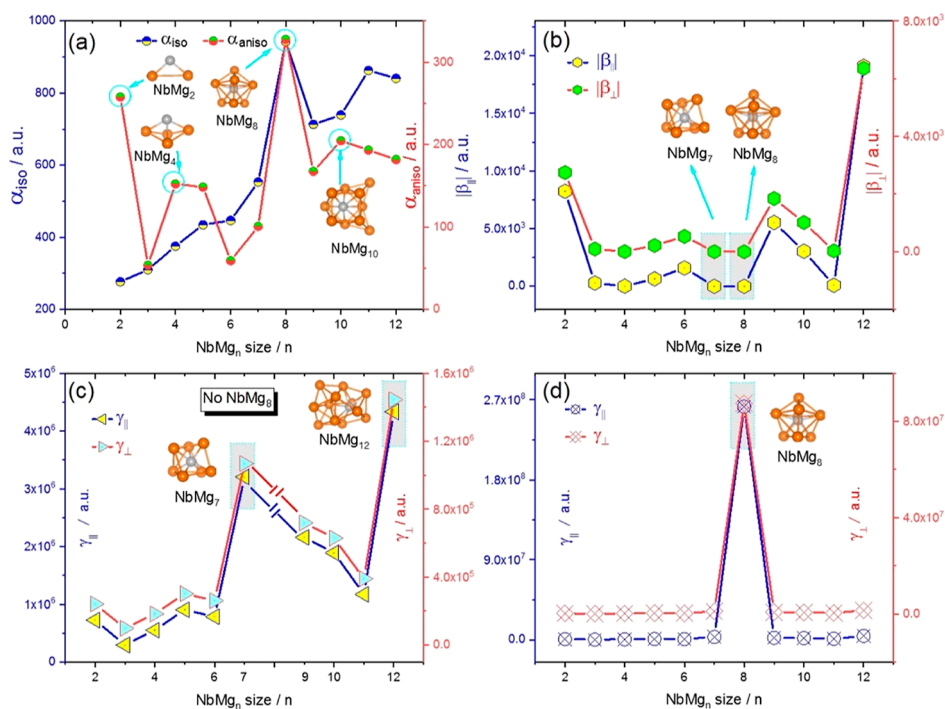


Figure 6. Polarizability and hyperpolarizability under electrostatic field for NbMg_n ($n = 2–12$) ground-state clusters: (a) Isotropy and anisotropy (α) for polarizability, (b) first hyperpolarizability for β_{\parallel} and β_{\perp} , (c) second hyperpolarizability (γ_{\parallel} and γ_{\perp}) without NbMg₈, and (d) second hyperpolarizability (γ_{\parallel} and γ_{\perp}) with NbMg₈.

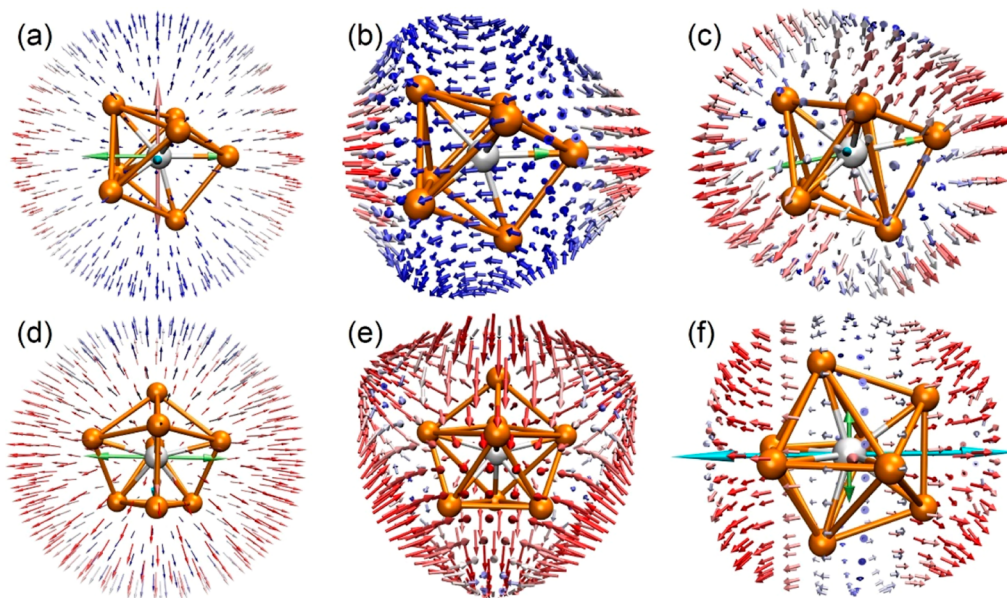


Figure 7. Unit sphere representation of the polarizability and hyperpolarizability tensor: (a) α , (b) β , and (c) γ for NbMg_n, and (d) α , (e) β , and (f) γ for NbMg₈.

cluster stability. Table 1 and Figure S3 in the Supporting Information show that the NbMg₂ ground-state isomer possesses the largest F-gap value (4.51 eV), followed by NbMg₃ (4.29 eV). Locally, the NbMg₅, NbMg₈, and NbMg₁₀ ground-state isomers have a larger F-gap than their neighbors. It is shown that the trends of KS-gap and F-gap curves with cluster size are overall decreasing but are different in the NbMg₅–NbMg₉ interval.

The above study shows that the ground-state isomer of the NbMg₈ cluster exhibits relatively superior relative stability.

When Mg₈ doped with another atom (X) in the magnesium-based clusters (XMg₈), it is found to exhibit high stability has also been reported in other studies. For example, Si, Ge, and Sn-doped^{69,70} Mg₈ all exhibit similar structures and high stability. However, it is worth noting that the structures of these isomers are different from that of the NbMg₈ ground-state isomer, as shown in this study.

3.3. Charge Transfer Characteristics Analysis of NbMg_n ($n = 2–12$) Clusters. In this work, the results of natural charge population (NCP) and natural electron

configuration (NEC) on Nb and Mg atoms in NBO calculations are shown in Tables 2, S2 and S3 in the Supporting Information. Figure 3 visualizes the NCP and NEC of the lowest-energy isomers of the Nb and Mg atoms of the NbMg_n ($n = 2-12$) cluster. As shown in Figure 3a, in all clusters, Nb atoms, in the range of -0.58 to -7.68 e, are gained electrons, while all Mg atoms play the role of losing electrons in the range of $0.09-1.04$ e. The character of charge transfer between Nb and Mg atoms in the NbMg_n ($n = 2-12$) ground-state isomer clusters derives from their electronegativity since the electronegativity value of the Mg atom is 1.31, whereas that of the Nb atoms is 1.6, and so the Nb atom attracts electrons more readily.

The NECs of Nb and Mg atoms reflect the number of specific orbital electrons, as can be seen from Tables 2, S2 and S3 in the Supporting Information, where Mg atoms gain and lose electrons mainly in the 3s and 3p valence orbitals, with occasional electron transfers to the 4s, 3d, and 4p orbitals; in a few clusters, atoms undergo electron transfers in the 5s, 4d, and 5p valence orbitals, all but NbMg₂ clusters gain a small number of electrons in the 5d orbital, and most clusters gain electrons in the 6p orbital (see Figure 3b). Specifically, Mg atoms in all clusters lose electrons in the 3s orbitals in the range of -0.33 to -1.14 e, and all other orbitals are electron gainers, whereas Nb atoms gain electrons in the 4d, 5p, 5d, and 6p orbitals, and the 5s orbitals of Nb atoms gain electrons in all clusters, except for a small number of electrons lost in NbMg₂ (0.09 e) and NbMg₆ (0.11 e). These results indicate that during the formation of the NbMg_n ($n = 2-12$) ground-state isomer clusters, the 3s orbitals of the Mg atoms are the “home base” for electron transfer, and most of them are transferred to the valence orbitals of the Nb atoms, which results in the emergence of the sp-hybridized orbitals of the Mg atoms and the spd-hybridized orbitals of the Nb atom.

3.4. IR and Raman Spectra of NbMg_n ($n = 2-12$) Clusters. IR and Raman spectra are closely related to the structural and vibrational states of clusters and are also experimentally directly detectable spectra. Therefore, here we have further predicted the IR and Raman spectra of all ground states of NbMg_n ($n = 2-12$) clusters by theoretical calculations. The positions of the six peaks with high relative intensities of IR and Raman for the NbMg_n ($n = 2-12$) ground-state isomers are shown in Table S4 of the Supporting Information and then plotted in Figures 4 and 5. The IR and Raman spectra of the NbMg₂ cluster have only single peaks at 195 and 188 cm⁻¹, respectively. For the NbMg₃ cluster, its strongest IR peak appears at 94 cm⁻¹, while the strongest Raman peak can be found at 213 cm⁻¹. Moreover, as shown in Table S4, two strong IR peaks and three Raman peaks appear at 186, 134, 136, 186, and 94 cm⁻¹, respectively. The calculations show that the strongest IR peak and the strongest Raman peak of the NbMg₄ cluster can be detected at 221 and 64 cm⁻¹. In addition, there are five additional IR peaks and three Raman peaks distributed between 94 and 221 cm⁻¹. The strongest IR and Raman peaks of the NbMg₅ cluster can be detected at 262 and 218 cm⁻¹, respectively. Another five strong Raman and four IR peaks can be found in the range of 44–262 cm⁻¹. The strongest IR peak of the NbMg₆ cluster appears at 117 cm⁻¹, while its strongest Raman peak appears at 233 cm⁻¹. Two more subintense Raman peaks of NbMg₆ can be found at 286 and 70 cm⁻¹, while five stronger IR peaks can be found in a larger frequency band (12–304 cm⁻¹). The strongest IR and Raman peaks of the NbMg₇ cluster appear at 109 and 249

cm⁻¹, the second and third strongest IR peaks can be found at 244 and 324 cm⁻¹, while the other three strong Raman peaks appear at 94, 129, and 324 cm⁻¹, respectively. Both the IR and Raman strongest peaks of the NbMg₈ cluster appear at 190 cm⁻¹, and the other two IR and four Raman strong peaks are distributed in the band from 30 to 297 cm⁻¹. Both IR and Raman spectra of NbMg₉ clusters show several strong peaks in the 400 cm⁻¹ band, where the strongest IR and Raman peaks can be detected at 285 and 228 cm⁻¹, and the remaining five Raman and IR peaks are distributed in the frequency band from 124 to 316 cm⁻¹. The IR and Raman strongest peaks of NbMg₁₀ and NbMg₁₂ clusters are coincident, and they are located at 274 and 276 cm⁻¹, respectively, while the strongest IR and Raman peaks of NbMg₁₁ can be detected at 248 and 197 cm⁻¹, respectively. Multiple strong IR and Raman peaks of these three clusters are also detected in the frequency band from 82 to 306 cm⁻¹.

All the IR and Raman strong peaks of the ground-state isomer of the NbMg_n cluster are distributed in the far-IR region less than 400 cm⁻¹, while the three strongest peaks are mainly distributed in the range of 100–300 cm⁻¹, as shown in the last subplot of Figure 5. This indicates that it is still difficult to directly detect by IR and Raman spectroscopy.

3.5. Linear and Nonlinear Optical Properties of NbMg_n ($n = 2-12$) Clusters. Because of their structural diversity, atomic clusters often exhibit special optical properties that are worth studying. As the last part of the study, the permanent dipole moment (μ_0), polarizability (α), first and second hyperpolarizability (β and γ) for each size NbMg_n ($n = 2-12$) ground-state isomer under a static external electric field are calculated to investigate their linear and NLO characteristics. The corresponding μ_0 , α , β , and γ formulas and results are presented in Table S5 of the Supporting Information. As shown in Table S5–2 and Figure S4 in the Supporting Information, the dipole moment calculations for NbMg_n show that μ_0 is not zero for all clusters, except for the NbMg₈ cluster, and this result is consistent with the conclusion of cluster point group symmetry (presented in Figure 1). It is noteworthy that NbMg₈ does not have a permanent dipole moment, indicating that it is the only one that has a totally symmetric electrically neutral cluster. The linear optical properties are described by the isotropic α_{iso} and anisotropic α_{aniso} of the static polarization tensor α , while the second-order β and third-order γ NLO parameters allow the NLO properties of the clusters to be studied. It is important to explain that Figures 6 and S5 in the Supporting Information show curves of the values of these polarizability quantities (α , β , and γ) corresponding to specific directions with cluster size, while Figures 7 and S6 in the Supporting Information plot more visually the unit sphere representation of the optical coefficients of all clusters. The color change of the arrows in the figures of the unit sphere representation follows a blue–white–red variation, with shorter arrows being bluer and longer arrows being redder, indicating their corresponding larger polarizability values.

As shown in Figure 6a and Table S5–1 in the Supporting Information, the α_{iso} of NbMg_n clusters overall increases with increasing cluster size, but the isotropic linear optical parameter (α_{iso}) of NbMg₈ (943.22) clusters is the largest one compared to all other clusters, indicating that it has the most pronounced linear response to optics under electrostatic field conditions. While the α_{aniso} curves oscillate with increasing cluster size, the three local maxima appear at the NbMg₂ (257.92), NbMg₄ (152.24), and NbMg₈ (327.72) clusters,

respectively. This implies that the linear optical response of these three clusters to the electrostatic field in different directions has a more significant difference compared to that of other clusters, with the most intense in the NbMg₈ cluster. To demonstrate this optical property more visually, Figures 7 and S6 in the Supporting Information also show the unit sphere representation of all clusters α . For the second-order nonlinear coefficients, the variation of the absolute value quantities in the parallel (β_{\parallel}) and perpendicular directions (β_{\perp}), respectively μ_0 , is presented. It is obvious that both β_{\parallel} and β_{\perp} for NbMg₈ are zero, indicating that its NLO response remains insensitive in the second-order fine structure. NbMg₇ has the second smallest β_{\parallel} and β_{\perp} values, but it has great polarizability in the x direction, indicating that it has a sensitive NLO response in this reverse direction, which is directly demonstrated in Figure 7b. Interestingly, the third-order NLO coefficient calculation shows that both γ_{\parallel} and γ_{\perp} of the NbMg₈ cluster exhibit an extremely excellent NLO response, which can be directly related to its hyperfine structure. Figure 7c,d shows that the NbMg₈ cluster possesses extremely large values of the third-order NLO coefficient γ , followed by NbMg₁₂ and NbMg₇. Figure 7f, on the other hand, shows that the γ values of the NbMg₈ cluster appear light blue only in a very small direction, indicating that it is sensitive to the NLO response in most directions. Furthermore, the unit sphere representation of Figure S6 in the Supporting Information with regard to α , β , and γ shows that the NbMg₅ cluster has the best isotropy of linear and NLO features, followed by the NbMg₃ cluster. In addition, the μ_0 , α , β , and γ curves in all directions shown in Figure S5 in the Supporting Information further confirm that the NbMg₈ cluster appears to be very special.

In conclusion, the ground-state isomer of the NbMg₈ cluster possesses the most fascinating optical properties. Because, although it does not have a permanent dipole moment and its linear optical response and second order NLO coefficients show no special properties, its third-order NLO response is extremely excellent in one direction, indicating that it is a powerful candidate for a potentially ultrasensitive NLO response device.

4. CONCLUSIONS

Using CALYPSO and GAUSSIAN code, NbMg_{*n*} ($n = 2-12$) gas-phase clusters are fully studied in this work. The structural growth mode study reveals that NbMg_{*n*} ($n = 2-12$) clusters are growing based on the seed of tetrahedral and pentahedral structures. Stability calculations for several parameters indicate that the relative stability of the ground state of the NbMg₈ cluster is outstanding. Charge transfer characteristics of Nb and Mg atoms were fully studied. Infrared and Raman spectra are theoretically calculated in detail in order to give guidance for future experimental probes. Finally, the linear and NLO response properties of the ground-state isomers of NbMg_{*n*} ($n = 2-12$) under a static electric field were explored by calculating and plotting the static polarizability and hyperpolarizability tensor. NbMg₈ was found to have excellent NLO properties and is a strong candidate for the future development of Nb-doped magnesium cluster-based assembled nano-optical materials.

■ ASSOCIATED CONTENT

SI Supporting Information

The Supporting Information is available free of charge at <https://pubs.acs.org/doi/10.1021/acsomega.3c05113>.

Structural coordinate, charge and spin multiplicity in the lowest-energy isomers of NbMg_{*n*} ($n = 2-12$) clusters, NCP and NEC of Mg atoms in the lowest-energy isomers of NbMg_{*n*} ($n = 2-12$) clusters, six strong IR and Raman peaks of the lowest-energy isomers of NbMg_{*n*} ($n = 2-12$) clusters, the polarizability and hyperpolarizability tensor and permanent dipole moment in the lowest-energy isomers of NbMg_{*n*} ($n = 2-12$) clusters, two unit structure seeds for the clusters' growth, the E_{gap} for β -electrons in the lowest-energy isomers of NbMg_{*n*} ($n = 2-12$) clusters, KS-gap and F-gap in the lowest-energy isomers of NbMg_{*n*} ($n = 2-12$) clusters, permanent dipole moment (μ_0) curve of NbMg_{*n*} ($n = 2-12$) ground-state isomers, variation curves of the values of μ_0 , α , β , and γ in the xyz direction with cluster size, and the unit spherical representation of the polarization and hyperpolarization tensor (PDF)

■ AUTHOR INFORMATION

Corresponding Authors

Ben-Chao Zhu – School of Public Health, Hubei University of Medicine, Shiyan 442000, People's Republic of China; orcid.org/0000-0002-6028-2017;
Email: benchao_zhu@126.com

Ding-Shan Zheng – School of Physics and Optoelectronic Engineering, Yangtze University, Jingzhou 434023, People's Republic of China; Email: dszheng82@163.com

Yan-Hua Liao – School of Mathematics and Physics, Hubei Polytechnic University, Huangshi 435003, People's Republic of China; orcid.org/0000-0002-3262-354X;
Email: liaoyanhua@whu.edu.cn

Authors

Xiao-Feng Gao – School of Mathematics and Physics, Hubei Polytechnic University, Huangshi 435003, People's Republic of China; School of Physics and Optoelectronic Engineering, Yangtze University, Jingzhou 434023, People's Republic of China

Guang-Hui Liu – Daye Special Steel Co., LTD, Huangshi 435003, People's Republic of China

Xian-Kai Hu – School of Mathematics and Physics, Hubei Polytechnic University, Huangshi 435003, People's Republic of China

Lan-Li Chen – School of Mathematics and Physics, Hubei Polytechnic University, Huangshi 435003, People's Republic of China; orcid.org/0000-0002-4552-9034

Complete contact information is available at:

<https://pubs.acs.org/doi/10.1021/acsomega.3c05113>

Author Contributions

X.-F.G.: Writing, original draft preparation, and methodology. **G.-H.L.:** Formal analysis and visualization. **X.-K.H.:** Formal analysis and visualization. **L.-L.C.:** Visualization. **B.-C.Z.:** Software, conceptualization, and writing review. **D.-S.Z.:** Software, methodology, and writing review. **Y.-H.L.:** Conceptualization, methodology, investigation, writing review, and editing.

Notes

The authors declare no competing financial interest.

ACKNOWLEDGMENTS

Y.-H.L. acknowledges the support from the Natural Science Foundation of Hubei Province grant no. 2022CFD056 and the Teaching Research Program of Education Department of Hubei Province grant no. 2020660. L.-L.C. acknowledges the support from the National Natural Science Foundation of China grant no. 52002123. B.-C.Z. acknowledges the support from Open Project of State Key Laboratory of Superhard Materials, Jilin University, grant no. 202317.

REFERENCES

- (1) Jena, P.; Castleman, A. W. Chapter 1 - Introduction to Atomic Clusters. In *Sci. Technol. At. Mol. Condens. Matter Biol. Syst.*; Jena, P., Castleman, A. W., Eds.; Elsevier, 2010; pp 1–36.
- (2) Solov'yov, I. A.; Korol, A. V.; Solov'yov, A. V. Atomic Clusters and Nanoparticles. In *Multiscale Model. Complex Mol. Struct. Dyn. MBN Explor.*; Solov'yov, I. A., Korol, A. V., Solov'yov, A. V., Eds.; Springer International Publishing: Cham, 2017; pp 121–170.
- (3) Pal, R.; Poddar, A.; Chattaraj, P. K. Atomic Clusters: Structure, Reactivity, Bonding, and Dynamics. *Front. Chem.* **2021**, *9*, 730548.
- (4) Rao, B. K. Atomic clusters — a possible source for novel materials. *Mater. Sci. Eng., A* **2001**, *304–306*, 211–214.
- (5) Jena, P.; Sun, Q. Super Atomic Clusters: Design Rules and Potential for Building Blocks of Materials. *Chem. Rev.* **2018**, *118*, 5755–5870.
- (6) Häkkinen, H. Atomic and electronic structure of gold clusters: understanding flakes, cages and superatoms from simple concepts. *Chem. Soc. Rev.* **2008**, *37*, 1847–1859.
- (7) Xu, W. W.; Zhu, B.; Zeng, X. C.; Gao, Y. A grand unified model for liganded gold clusters. *Nat. Commun.* **2016**, *7*, 13574.
- (8) Fournier, R. Theoretical study of the structure of silver clusters. *J. Chem. Phys.* **2001**, *115*, 2165–2177.
- (9) Alameddine, G.; Hunter, J.; Cameron, D.; Kappes, M. M. Electronic and geometric structure in silver clusters. *Chem. Phys. Lett.* **1992**, *192*, 122–128.
- (10) Aguilera-Granja, F.; Piotrowski, M. J.; da Silva, J. L. F. Structural and electronic properties of $\text{TM}_{23-p}\text{Ag}_p$ (TM = Ni, Pd, and Pt) clusters in the dilute limit ($p = 0–4$): A density functional theory investigation. *Eur. Phys. J. D* **2013**, *67*, 33.
- (11) Aguilera-Granja, F.; Vega, A.; Gallego, L. J. A density-functional study of the structures, binding energies and magnetic moments of the clusters Mo_N ($N = 2–13$), Mo_{12}Fe , Mo_{12}Co and Mo_{12}Ni . *Nanotechnology* **2008**, *19*, 145704.
- (12) Aguilera-Granja, F.; Longo, R. C.; Gallego, L. J.; Vega, A. Structural and magnetic properties of X_{12}Y ($X, Y = \text{Fe, Co, Ni, Ru, Rh, Pd, and Pt}$) nanoalloys. *J. Chem. Phys.* **2010**, *132*, 184507.
- (13) Aguilera-Granja, F.; Vega, A. Stability, magnetic behavior, and chemical order of $(\text{Co}_x\text{Fe}_{1-x})_N$ ($N = 5, 13$) nanoalloys. *Phys. Rev. B* **2009**, *79*, 144423.
- (14) Montejano-Carrizales, J. M.; Aguilera-Granja, F.; Goyhenex, C.; Pierron-Bohnes, V.; Morán-López, J. Structural, electronic and magnetic properties of $\text{Co}_n\text{Pt}_{M-n}$, for $M = 13, 19$, and 55 , from first principles. *J. Magn. Magn. Mater.* **2014**, *355*, 215–224.
- (15) Varas, A.; Aguilera-Granja, F.; Rogan, J.; Kiwi, M. Structural, electronic, and magnetic properties of $\text{Fe}_x\text{Co}_y\text{Ni}_z$ ($x+y+z = 13$) clusters: A density-functional-theory study. *J. Magn. Magn. Mater.* **2015**, *394*, 325–334.
- (16) Varas, A.; Aguilera-Granja, F.; Rogan, J.; Kiwi, M. Structural, electronic, and magnetic properties of $\text{Fe}_x\text{Co}_y\text{Pd}_z$ ($x + y + z \leq 7$) clusters: a density functional theory study. *J. Nanopart. Res.* **2016**, *18*, 252.
- (17) Jug, K.; Zimmermann, B.; Calaminici, P.; Köster, A. M. Structure and stability of small copper clusters. *J. Chem. Phys.* **2002**, *116*, 4497–4507.
- (18) Wang, X.; Wang, H.; Luo, Q.; Yang, J. Structural and electrocatalytic properties of copper clusters: A study via deep learning and first principles. *J. Chem. Phys.* **2022**, *157*, 074304.
- (19) Song, W.; Lu, W.-C.; Wang, C. Z.; Ho, K. M. Magnetic and electronic properties of the nickel clusters Ni_n ($n \leq 30$). *Comput. Theor. Chem.* **2011**, *978*, 41–46.
- (20) Goel, S.; Masunov, A. E. Density functional theory study of small nickel clusters. *J. Mol. Model.* **2012**, *18*, 783–790.
- (21) Aguilera-Granja, F.; Gallego, L. J. Structural and electronic properties of $\text{Ni}_{26-p}\text{X}_p$ clusters ($X = \text{Pd, Pt}$): A density-functional-theoretic study. *J. Appl. Phys.* **2013**, *114*, 054311.
- (22) Jellinek, J.; Acioli, P. H. Magnesium Clusters: Structural and Electronic Properties and the Size-Induced Nonmetal-to-Metal Transition. *J. Phys. Chem. A* **2002**, *106*, 10919–10925.
- (23) Xia, X.; Kuang, X.; Lu, C.; Jin, Y.; Xing, X.; Merino, G.; Hermann, A. Deciphering the Structural Evolution and Electronic Properties of Magnesium Clusters: An Aromatic Homonuclear Metal Mg_{17} Cluster. *J. Phys. Chem. A* **2016**, *120*, 7947–7954.
- (24) Liu, Z.; Lu, T.; Yuan, A.; Wang, X.; Chen, Q.; Yan, X. Remarkable Size Effect on Photophysical and Nonlinear Optical Properties of All-Carboatomic Rings, Cyclo[18]carbon and Its Analogues. *Chem.—Asian J.* **2021**, *16*, 2267–2271.
- (25) Liu, Z.; Lu, T.; Chen, Q. An sp-hybridized all-carboatomic ring, cyclo[18]carbon: Bonding character, electron delocalization, and aromaticity. *Carbon* **2020**, *165*, 468–475.
- (26) Liu, Z.; Lu, T.; Chen, Q. An sp-hybridized all-carboatomic ring, cyclo[18]carbon: Electronic structure, electronic spectrum, and optical nonlinearity. *Carbon* **2020**, *165*, 461–467.
- (27) Chen, B.; Gutsev, G. L.; Li, D.; Ding, K. Structure and Chemical Bonding in Medium-Size Boron Clusters Doped with Praseodymium. *Inorg. Chem.* **2022**, *61*, 7890–7896.
- (28) Avdeeva, V. V.; Malinina, E. A.; Kuznetsov, N. T. Boron cluster anions and their derivatives in complexation reactions. *Coord. Chem. Rev.* **2022**, *469*, 214636.
- (29) Tekin, A.; Hartke, B. Global geometry optimization of small silicon clusters with empirical potentials and at the DFT level. *Phys. Chem. Chem. Phys.* **2004**, *6*, 503–509.
- (30) Pouchan, C.; Bégué, D.; Zhang, D. Y. Between geometry, stability, and polarizability: Density functional theory studies of silicon clusters Si_n ($n = 3–10$). *J. Chem. Phys.* **2004**, *121*, 4628–4634.
- (31) Álvarez-Zapatero, P.; Lebon, A.; Aguilera del Toro, R. H.; Aguado, A.; Vega, A. Why are Zn-rich Zn–Mg nanoalloys optimal protective coatings against corrosion? A first-principles study of the initial stages of the oxidation process. *Phys. Chem. Chem. Phys.* **2021**, *23*, 24685–24698.
- (32) Zhang, J.; Glezakou, V.-A. Global optimization of chemical cluster structures: Methods, applications, and challenges. *Int. J. Quantum Chem.* **2021**, *121*, No. e26553.
- (33) Zhang, J.; Dolg, M. Global optimization of clusters of rigid molecules using the artificial bee colony algorithm. *Phys. Chem. Chem. Phys.* **2016**, *18*, 3003–3010.
- (34) Lv, J.; Wang, Y.; Zhu, L.; Ma, Y. Particle-swarm structure prediction on clusters. *J. Chem. Phys.* **2012**, *137*, 084104.
- (35) Zhang, X.-Y.; Zhao, Y.-R.; Li, H.-X.; Cheng, K.-G.; Liu, Z.-R.; Liu, Z.-P.; He, H. Probing the effects of lithium doping on structures, properties, and stabilities of magnesium cluster anions. *Chin. Phys. B* **2023**, *32*, 066102.
- (36) Zhang, F.; Zhang, H.; Xin, W.; Chen, P.; Hu, Y.; Zhang, X.; Zhao, Y. Probing the structural evolution and electronic properties of divalent metal Be_2Mg_n clusters from small to medium-size. *Sci. Rep.* **2020**, *10*, 6052.
- (37) Liao, Y.-H.; Liu, G.-H.; Guo, J.; Dai, W.; Chen, S.-S.; Zhu, B.-C. Insights into the structural, electronic and spectral properties of gas-phase GaMg_n^+ ($n = 2–12$) clusters. *Optik* **2022**, *270*, 170093.
- (38) Zhu, B.-C.; Bao, L.; Deng, P.-J.; Zeng, L.; Kang, W.-B.; Guo, J. Systematic research on gallium atom-doped neutral small- and medium-sized gas-phase magnesium clusters: A DFT study of GaMg_n ($n = 2–12$) clusters. *J. Chem. Phys.* **2022**, *157*, 114303.
- (39) Liao, Y. H.; Zhou, W. L.; Lyon, J. T.; Peng, F.; Lu, C. The structure of anionic NbH_n^- ($n = 2–15$) clusters and their maximum hydrogen capacity. *New J. Phys.* **2022**, *24*, 043038.

- (40) Zhu, B.-C.; Liu, G.-H.; Deng, P.-J.; Liu, C.-J.; Liao, Y.-H.; Zeng, L.; Zhao, J. Study of the hydrogen absorption behaviour of a “number-sensitive” Mg atom: ultra-high hydrogen storage in MgH_n ($n = 1-20$) clusters. *J. Mater. Chem. A* **2023**, *11*, 13774–13782.
- (41) Li, C.-G.; Gao, J.-H.; Zhang, J.; Song, W.-T.; Liu, S.-Q.; Gao, S.-Z.; Ren, B.-Z.; Hu, Y.-F. Structures, stabilities and electronic properties of boron-doped silicon clusters B_3Si_n ($n = 1-17$) and their anions. *Mol. Phys.* **2019**, *117*, 382–394.
- (42) Liu, Y.; Yang, J.; Li, S.; Cheng, L. Structural growth pattern of neutral and negatively charged yttrium-doped silicon clusters $\text{YSi}_n^{0/-}$ ($n = 6-20$): from linked to encapsulated structures. *RSC Adv.* **2019**, *9*, 2731–2739.
- (43) Yan, L. Expanded spherical trihedral metallo-borosphenes of transition-metal doped boron clusters: $\text{TM}_3\text{B}_{15}^q$ ($\text{TM} = \text{Zr}, \text{Hf}; q = -1, 0, +1$). *Results Phys.* **2022**, *33*, 105214.
- (44) Li, C.-G.; Cui, Y.-Q.; Tian, H.; Zhang, J.; Shen, Z.-G.; Ren, B.-Z.; Yuan, Y.-Q. Study on structures, electronic, spectral and thermodynamic properties of lanthanide-doped boron-based MB_n^- ($M = \text{La}, \text{Ce}, \text{Pr}; n = 8, 9$) clusters. *J. Mol. Struct.* **2022**, *1256*, 132566.
- (45) Nico, C.; Monteiro, T.; Graça, M. Niobium oxides and niobates physical properties: Review and prospects. *Prog. Mater. Sci.* **2016**, *80*, 1–37.
- (46) Prasad, S. V. S.; Prasad, S. B.; Verma, K.; Mishra, R. K.; Kumar, V.; Singh, S. The role and significance of Magnesium in modern day research-A review. *J. Magnesium Alloys* **2022**, *10*, 1–61.
- (47) Song, J.; She, J.; Chen, D.; Pan, F. Latest research advances on magnesium and magnesium alloys worldwide. *J. Magnesium Alloys* **2020**, *8*, 1–41.
- (48) Wang, Y.; Lv, J.; Zhu, L.; Ma, Y. CALYPSO: A method for crystal structure prediction. *Comput. Phys. Commun.* **2012**, *183*, 2063–2070.
- (49) Shao, X.; Lv, J.; Liu, P.; Shao, S.; Gao, P.; Liu, H.; Wang, Y.; Ma, Y. A symmetry-orientated divide-and-conquer method for crystal structure prediction. *J. Chem. Phys.* **2022**, *156*, 014105.
- (50) Lu, C.; Gong, W.; Li, Q.; Chen, C. Elucidating Stress-Strain Relations of ZrB_{12} from First-Principles Studies. *J. Phys. Chem. Lett.* **2020**, *11*, 9165–9170.
- (51) Li, H. X.; Cheng, K. G.; Wang, J. C.; Liu, Z. P.; He, H.; Zhao, Y. R. Probing the structural evolution, electronic and vibrational properties of anionic sodium-doped magnesium clusters. *Comput. Mater. Sci.* **2023**, *226*, 112212.
- (52) Zhao, Y.; Xu, Y.; Chen, P.; Yuan, Y.; Qian, Y.; Li, Q. Structural and electronic properties of medium-sized beryllium doped magnesium BeMg_n clusters and their anions. *Results Phys.* **2021**, *26*, 104341.
- (53) Guo, S.; Zhang, Y.; Wang, P.; Tang, H.; Dai, W.; Li, G.; Bi, J.; Zhu, B. Insights into the structural evolution and electronic properties of deficient-electron sodium chloride clusters. *Mater. Express* **2020**, *10*, 1404–1411.
- (54) Zhu, B.-C.; Deng, P.-J.; Guo, J.; Kang, W.-B.; Bao, L. Rapid 3D roll-up of gas-phase planar gold clusters and affinity and alienation for Mg and Ge: A theoretical study of MgGeAu_n ($n = 1-12$) clusters. *iScience* **2022**, *25*, 105215.
- (55) Wang, J.-W.; Lv, L.-X.; Liang, H.; Zhang, S.; Dai, W.; Zhu, B.-C. Structural and electronic properties of halogen (X)-doped aluminium clusters. *Chem. Phys. Lett.* **2020**, *757*, 137870.
- (56) Wu, J.-B.; Guo, J.; Zeng, L.; Zhang, S.; Zhu, B.-C. Computational probe for the geometrical structure and spectroscopic properties of Ga_2Mg_n^+ ($n = 1-11$) clusters. *Comput. Theor. Chem.* **2021**, *1206*, 113500.
- (57) Sun, W.; Chen, B.; Li, X.; Peng, F.; Hermann, A.; Lu, C. Ternary Na-P-H superconductor under high pressure. *Phys. Rev. B* **2023**, *107*, 214511.
- (58) Duan, Q.; Shen, J.; Zhong, X.; Lu, H.; Lu, C. Structural phase transition and superconductivity of ytterbium under high pressure. *Phys. Rev. B* **2022**, *105*, 214503.
- (59) Becke, A. D. Density-functional thermochemistry. I. The effect of the exchange-only gradient correction. *J. Chem. Phys.* **1992**, *96*, 2155–2160.
- (60) Krishnan, R.; Binkley, J. S.; Seeger, R.; Pople, J. A. Self-consistent molecular orbital methods. XX. A basis set for correlated wave functions. *J. Chem. Phys.* **1980**, *72*, 650–654.
- (61) Frisch, M. J.; Trucks, G. W.; Schlegel, H. B.; Scuseria, G. E.; Robb, M. A.; Cheeseman, J. R.; Scalmani, G.; Barone, V.; Petersson, G. A.; Nakatsuji, H.; Li, X.; Caricato, M.; Marenich, A.; Bloino, J.; Janesko, B. G.; Gomperts, R.; Mennucci, B.; Hratchian, H. P.; Ortiz, J. V.; Izmaylov, A. V.; Sonnenberg, J. L.; Williams-Young, D.; Ding, F.; Lipparini, F.; Egidi, F.; Goings, J.; Peng, B.; Petrone, A.; Henderson, T.; Ranasinghe, D.; Zakrzewski, V. G.; Gao, J.; Rega, N.; Zheng, J.; Liang, W.; Hada, M.; Ehara, M.; Toyota, K.; Fukuda, R.; Hasegawa, J.; Ishida, M.; Nakajima, T.; Honda, Y.; Kitao, O.; Naka, H.; Vreven, T.; Throssell, K.; Montgomery, J. E., Jr; Peralta, J. E.; Ogliaro, F.; Bearpark, M.; Heyd, J. J.; Brothers, E.; Kudin, K. N.; Staroverov, V. N.; Keith, T.; Kobayashi, R.; Normand, J.; Raghavachari, K.; Rendell, A.; Burant, J. C.; Iyengar, S. S.; Tomasi, J.; Cossi, M.; Millam, J. M.; Klene, M.; Adamo, C.; Cammi, R.; Ochterski, J. W.; Martin, R. L.; Morokuma, K.; Farkas, O.; Foresman, J. B.; Fox, D. J. *Gaussian 09*. Revision A.02, 2016. <https://gaussian.com/g09citation/>.
- (62) Pritchard, B. P.; Altaraw, D.; Didier, B.; Gibson, T. D.; Windus, T. L. New Basis Set Exchange: An Open, Up-to-Date Resource for the Molecular Sciences Community. *J. Chem. Inf. Model.* **2019**, *59*, 4814–4820.
- (63) Reed, A. E.; Weinstock, R. B.; Weinhold, F. Natural population analysis. *J. Chem. Phys.* **1985**, *83*, 735–746.
- (64) Grimme, S.; Ehrlich, S.; Goerigk, L. Effect of the damping function in dispersion corrected density functional theory. *J. Comput. Chem.* **2011**, *32*, 1456–1465.
- (65) Lu, T.; Chen, F. Multiwfn: A multifunctional wavefunction analyzer. *J. Comput. Chem.* **2012**, *33*, 580–592.
- (66) Zeng, L.; Wei, X.-F.; Liang, M.-K.; Deng, P.-J.; Bi, J.; Zhu, B.-C. BeMg_n: A tower-like type doped magnesium clusters with high stability. *Comput. Mater. Sci.* **2020**, *182*, 109795.
- (67) Ge, G.-X.; Han, Y.; Wan, J.-G.; Zhao, J.-J.; Wang, G.-H. First-principles prediction of magnetic superatoms in 4d-transition-metal-doped magnesium clusters. *J. Chem. Phys.* **2013**, *139*, 174309.
- (68) Baerends, E. J.; Gritsenko, O. V.; van Meer, R. The Kohn–Sham gap, the fundamental gap and the optical gap: the physical meaning of occupied and virtual Kohn–Sham orbital energies. *Phys. Chem. Chem. Phys.* **2013**, *15*, 16408–16425.
- (69) Zeng, L.; Liang, M.-K.; Wei, X.-F.; Guo, J.; Dai, W.; Zhu, B.-C. New potential stable structures of XMg_n ($X = \text{Ge}, \text{C}, \text{Sn}; n = 2-12$) clusters: XMg_8 with high stability. *J. Phys.: Condens. Matter* **2021**, *33*, 065302.
- (70) Zhu, B.-C.; Zhang, S.; Zeng, L. The effect of silicon doping on the geometrical structures, stability, and electronic and spectral properties of magnesium clusters: DFT study of SiMg_n ($n = 1-12$) clusters. *Int. J. Quantum Chem.* **2020**, *120*, No. e26143.